7-1-2021

Early corn stand count of different cropping systems using UAV-imagery and deep learning

Chin Nee Vong
University of Missouri

Lance S. Conway
University of Missouri

Jianfeng Zhou
University of Missouri, zhoujianf@missouri.edu

Newell R. Kitchen
USDA Agricultural Research Service

Kenneth A. Sudduth
USDA Agricultural Research Service

Computers and Electronics in Agriculture 186 (2021) 106214

Contents lists available at ScienceDirect

Computers and Electronics in Agriculture

journal homepage: www.elsevier.com/locate/compag

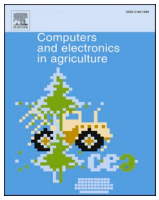

Original papers

Early corn stand count of different cropping systems using UAV-imagery and deep learning

Chin Nee Vong [a], Lance S. Conway [b], Jianfeng Zhou [a,*], Newell R. Kitchen [c], Kenneth A. Sudduth [c]

[a] Division of Food Systems and Bioengineering, University of Missouri, Columbia, MO 65211, USA
[b] Division of Soil, Environmental, and Atmospheric Sciences, University of Missouri, Columbia, MO 65211, USA
[c] USDA-ARS Cropping Systems & Water Quality Research Unit, Columbia, MO, 65211, USA

ARTICLE INFO

Keywords:
Corn
Cropping systems
Deep learning
Stand count
UAV imagery

ABSTRACT

Optimum plant stand density and uniformity is vital in order to maximize corn (*Zea mays* L.) yield potential. Assessment of stand density can occur shortly after seedlings begin to emerge, allowing for timely replant decisions. The conventional methods for evaluating an early plant stand rely on manual measurement and visual observation, which are time consuming, subjective because of the small sampling areas used, and unable to capture field-scale spatial variability. This study aimed to evaluate the feasibility of an unmanned aerial vehicle (UAV)-based imaging system for estimating early corn stand count in three cropping systems (CS) with different tillage and crop rotation practices. A UAV equipped with an on-board RGB camera was used to collect imagery of corn seedlings (~14 days after planting) of CS, i.e., minimum-till corn-soybean rotation (MTCS), no-till corn-soybean rotation (NTCS), and no-till corn-corn rotation with cover crop implementation (NTCC). An image processing workflow based on a deep learning (DL) model, U-Net, was developed for plant segmentation and stand count estimation. Results showed that the DL model performed best in segmenting seedlings in MTCS, followed by NTCS and NTCC. Similarly, accuracy for stand count estimation was highest in MTCS ($R^2 = 0.95$), followed by NTCS (0.94) and NTCC (0.92). Differences by CS were related to amount and distribution of soil surface residue cover, with increasing residue generally reducing the performance of the proposed method in stand count estimation. Thus, the feasibility of using UAV imagery and DL modeling for estimating early corn stand count is qualified influenced by soil and crop management practices.

1. Introduction

Optimum plant density and uniformity are critical crop management parameters to maximize crop production and yield, especially for corn (*Zea mays* L.) (Sangoi, 2001). Optimal plant density is determined based on a number of factors, such as hybrid, maturity, length of growing season, and planting date (Sangoi, 2001). For example, higher planting density is suggested for early planting where there is a risk of yield loss due to the lower soil and air temperature (Bollero et al., 1996; Sangoi, 2001; Stanger and Lauer, 2006). In addition, higher planting density is utilized to increase the stress-tolerance of corn hybrids to maximize yield (Assefa et al., 2016; Van Roekel and Coulter, 2011). Although seeds may be planted at the optimum density, spatial variation of the plant density can occur due to poor seed germination (including emergence delays and/or failed emergence), planter performance problems, and early-season plant death due to stress (Thorp et al., 2007). Collectively, this variability affects final corn grain yield. Therefore, early assessment of plant density by quantifying stand count is valuable for subsequent management decisions (e.g., replanting and post-emerge herbicide applications) and for evaluating spatial yield variability as shown in yield maps.

The conventional method for an early stand count is usually based on manually counting the number of seedlings at multiple sites within a given field (Nielsen, 2003). Manual assessment of stand count is time consuming, labor intensive, subjective due to small sampling areas used, and may not be representative of whole fields (Varela et al., 2018). In addition, sensors mounted on the row-dividers of a combine head have been developed to count and map plant density at harvest, resulting in more information for crop management recommendations for the next growing season (Birrell and Sudduth, 1995; Sudduth et al., 2000). However, this measurement has no value for guiding in-season management.

* Corresponding author.
E-mail address: zhoujianf@missouri.edu (J. Zhou).

https://doi.org/10.1016/j.compag.2021.106214
Received 28 January 2021; Received in revised form 28 April 2021; Accepted 13 May 2021
Available online 23 May 2021

Recently, UAV-based imaging systems have shown the potential of capturing high resolution red–green-blue (RGB) images for detecting and estimating stand counts of different crops including corn (Gnadinger and Schmidhalter, 2017; Kitano et al., 2019; Shuai et al., 2019; Varela et al., 2018), wheat (*Triticum aestivum* L.) (Jin et al., 2017), cotton (*Gossypium* L.) (Chen et al., 2018), rapeseed (*Brassica napus* L.) (Zhao et al., 2018), and sorghum (*Sorghum bicolor* L.) (Ghosal et al., 2019; Guo et al., 2018). These studies acquired images using high resolution RGB cameras at a low altitude (3 to 20 m) that resulted in a ground sampling distance (GSD) of 0.20 to 8.9 mm pixel^{-1}. Studies showed that UAV-based methods could estimate stand counts accurately with coefficients of determination (R^2) of 0.80 to 0.91, 0.56 to 0.84, 0.72 to 0.89, and 0.89 for wheat (Jin et al., 2017), sorghum (Ghosal et al., 2019; Guo et al., 2018), rapeseed (Zhao et al., 2018), and corn (Gnadinger and Schmidhalter, 2017), respectively.

One of the most important steps in the assessment of crop stand count using UAV imagery is to segment plants from images. The crop segmentation can be conducted using vegetation indices to signify the difference between crop and background. For example, a simple excess green vegetation index was used to segment corn plants from UAV images where there were only small amounts of residue on the soil surface (Shuai et al., 2019; Varela et al., 2018). Gnadinger and Schmidhalter (2017) used contrast enhancement and threshold value in two color spaces (i.e., HSV and L*a*b) for image segmentation to detect plants at the 3- to 5-leaf development stage, while Kitano et al. (2019) used a deep learning (DL) method to estimate plant density with different treatments (plant densities, flying heights, and growth stages). Although these studies demonstrated the potential of detecting plants and determining corn stand count at early growth stages using global thresholds, they focused on fields under traditional agriculture practices that included conventional or minimum tillage, where the image background was simple and dominated by soil. In recent years, conservation agriculture has become popular due to its potential for mitigating negative environmental impacts while maintaining desired yield (Conway et al., 2018; Hobbs et al., 2008; Nunes et al., 2018; Pittelkow et al., 2015; Yost et al., 2016). Conservation agriculture fields that include no-till (crop planting with minimum soil disturbance), cover crops, and diverse crop rotations (Hobbs et al., 2008; Pittelkow et al., 2015) have plant residues that make it difficult to identify early-stage plants for accurate evaluation of stand count. For UAV imagery stand count methods to be widely adoptable, the stand count assessment methods need to be evaluated for corn fields where conservation agriculture is practiced and where there is a more complex background. Based on our best knowledge, the performance of UAV-based method in stand count assessment for crops managed using conservation agriculture has not been evaluated.

Due to advances in image processing and deep learning (DL) techniques, it is now possible to process images with more complex backgrounds. Deep learning is a kind of machine learning (ML), which is composed of different functions (e.g., convolutions, pooling layers, and fully connected layers) to transform data in a hierarchical way, forming a "deeper" neural network model (Kamilaris and Prenafeta-Boldú, 2018). Deep learning techniques are more effective than conventional ML in identification of subtle differences in images due to their ability for feature learning from raw data and automatic feature extraction in the model. Deep learning has shown great potential in segmenting plants from the soil background using low-altitude UAV images (Fan et al., 2018; Fawakherji et al., 2019; Kitano et al., 2019; Trujillano et al., 2018; Zhang et al., 2020; Zhuang et al., 2018). The RGB color and multispectral images captured from a UAV have been used in a DL model to segment tobacco (*Nicotiana tabacum* L.) (Fan et al., 2018), corn (Fawakherji et al., 2019; Kitano et al., 2019; Trujillano et al., 2018), sugar beet (*Beta vulgaris* L.) (Fawakherji et al., 2019), and purple rapeseed leaves (Zhang et al., 2020). Moreover, RGB images collected from a camera mounted on an agricultural robot were used in a DL model to segment corn and sugar beet plants under different light conditions (Zhuang et al., 2018). All these studies used the same type of DL model known as a convolutional neural network (CNN), which is primarily used for pattern recognition within images (Albawi et al., 2017). The main architecture of CNN is formed by stacked layers of convolution, pooling, and fully-connected layers. The convolution layer extracts features automatically from each input image and the pooling layer reduces the dimensionality of the extracted features (Amara et al., 2017). Then, the fully-connected layer at the end utilizes the learned features to classify the input images. Examples of the CNN models used include U-Net for corn and purple rapeseed leaves segmentation (Kitano et al., 2019; Zhang et al, 2020), Segnet and VGG-UNet for corn and sugar beet classification (Fawakherji et al., 2019), and LeNet for corn classification (Trujillano et al., 2018).

With the promising results from using UAV imagery and DL modeling for segmenting images, the present study aimed to evaluate the feasibility of UAV-based imagery and a DL model for estimating early corn stand count in different cropping systems (CS). The specific objectives included: 1) to build a DL model for segmenting corn plants in different CS from UAV images; and 2) to build an image processing workflow for corn early stand count estimation.

2. Material and methodology

2.1. Experimental site

This study was conducted in 2019 at a research farm in the United States Department of Agriculture, Agricultural Research Service (USDA-ARS) Long-Term Agroecosystem Research (LTAR) network (Sadler et al., 2015) near Centralia, MO (39°13′48″ N, 92°7′14″ W). A detailed description and research history of the site have been reported previously (Conway et al., 2018; Yost et al., 2016). In the present study, a large-plot area (12 ha) and an adjacent 4-ha field were used (Fig. 1). The replicated plot area had 10 CS main plots with three replications. Each plot was 190 m by 20 m (0.4 ha). As indicated in Table 1, this study included two of the 10 CS, i.e., minimum-tillage corn-soybean rotation (MTCS, Fig. 1) and no-till corn-soybean rotation (NTCS, Fig. 1). These have been managed in this same rotation for >25 years. A third CS, no-till continuous corn with cover crops (NTCC) was implemented in the adjacent 4-ha field (Fig. 1). For MTCS and NTCS, the plots were planted with soybean (*Glycine* max) in 2018, resulting in low to medium amounts of residue in the plots when planting corn in 2019 (Fig. 2a-d). Meanwhile, in the spring of 2018, corn was planted in the NTCC, followed by a cover crop seeding in the fall. The cover crop consisted of cereal rye (*Secale cereale* L.) and hairy vetch (*Vicia villosa Roth*), causing a higher percentage of residue cover when planting in 2019 (Fig. 2e and f).

A 4-row planter with John Deere *MaxEmerge XP* row units (Deere & Co., Moline, IL, USA) was used for planting corn (hybrid Pioneer 0589, Corteva Agriscience, Wilmington, DE, USA) in all plots at a row spacing of 0.76 m. In 2019, MTCS and NTCS plots were planted on May 15, while the NTCC field was planted on May 31 (Table 1). Seeding rate was set as 81,510 seeds ha^{-1} across the site, which was equivalent to a plant spacing of 16 cm. Additionally, the planter was outfitted with a Precision Planting hydraulic downforce system (DeltaForce®) and finger-pickup seed meters (Precision Planting, LLC., Tremont, IL, USA). No planter residue management (e.g., row cleaners and no-till coulters) was used during the seeding operation.

2.2. UAV data collection

Aerial image data was collected using a Phantom 4 Advanced UAV (DJI, Shenzhen, Guangdong, China) equipped with an on-board RGB camera. The camera had a field-of-view (FOV) of 84° and the selected image size was 4864 by 3648 pixels. Imagery was taken about two weeks after planting when the corn was at the second leaf vegetative growth stage (V2) or earlier. Specifically, data were collected for the MTCS and NTCS plots on May 28 and the NTCC field on June 14, 2019 (Table 1).

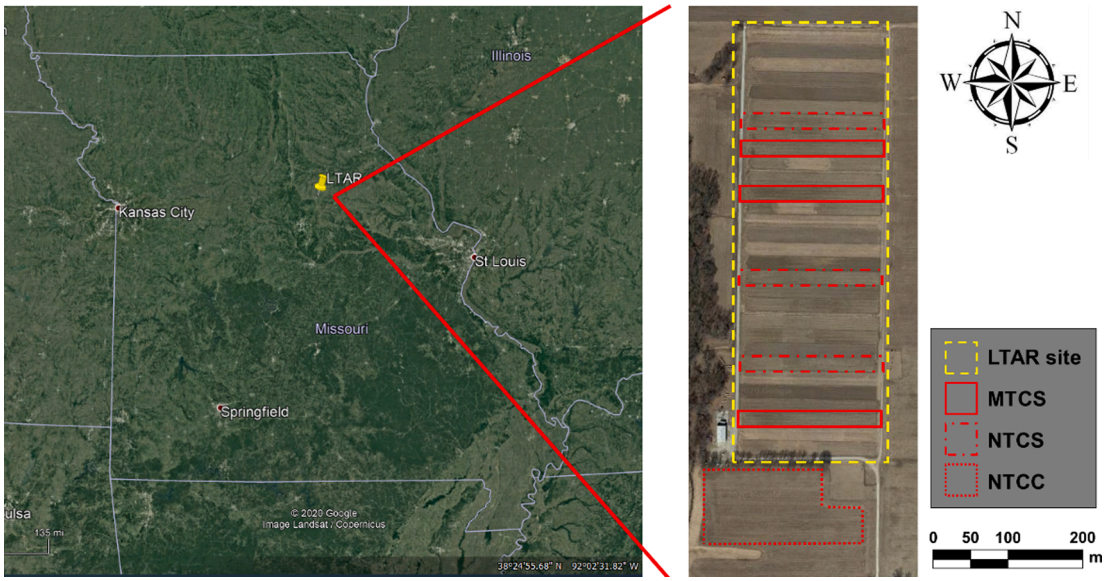

Fig. 1. Long-Term Agroecosystem Research (LTAR) experimental site used for this study with different cropping systems (MTCS: minimum-till corn-soybean; NTCS: no-till corn-soybean; NTCC: no-till corn-corn including cover crop) identified.

Table 1
Cropping system description, date of planting, and UAV image acquisition date in 2019 at the study site near Centralia, MO.

Cropping System	Description	Residue Cover	Planting Date	UAV Image Date
MTCS	Minimum-till; Corn following soybean	None/Low	May 15th	May 28th
NTCS	No-till; Corn following soybean	Medium	May 15th	May 28th
NTCC	No-till; Corn following corn with cover crops	High	May 31st	June 14th

Sequential images were taken at 0.5 frame per second (fps) at a 10-m flight height and a speed of 2 m s^{-1}, which were set by planning the mission waypoints using the UAV control app Litchi (VC Technology Ltd, London, U.K.) to ensure image overlap of 75% in both forward and sideward directions. Each image frame had a calculated ground sampling distance (GSD) of 0.3 cm $pixel^{-1}$ and covered an area of approximately 159.1 m^2 (14.6 m × 10.9 m). This resulted in about 19 corn rows per image.

2.3. Image processing and data analysis

Due to the complexity of images with small corn plants and heavy residues, as well as cover crops in the NTCC CS, an image processing method based on deep learning (DL) was used in this study to segment

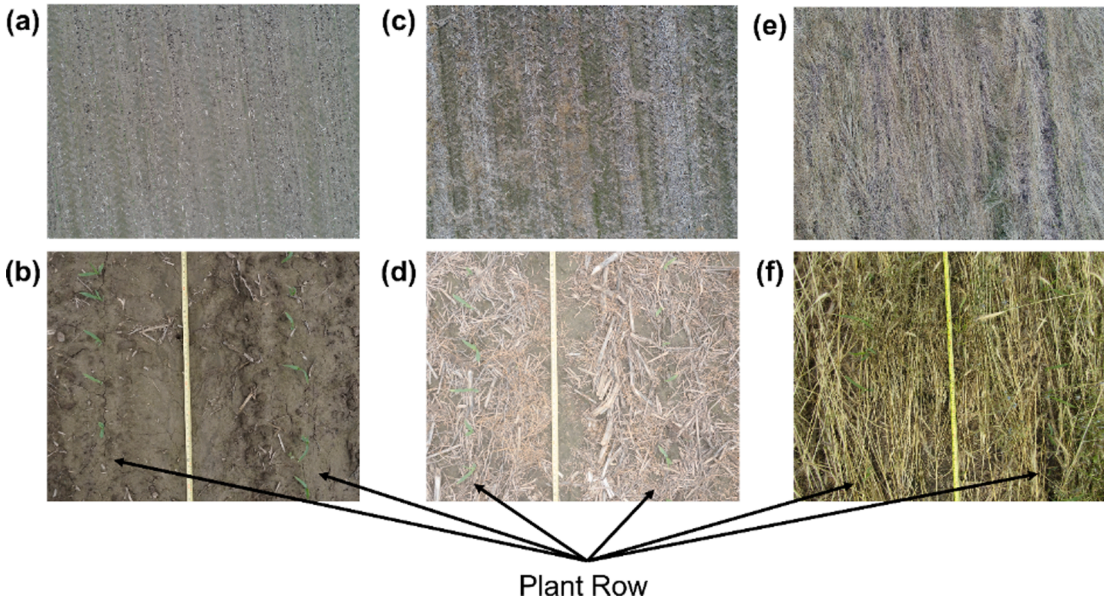

Fig. 2. Images of the three cropping systems with different types and amounts of residue cover. Images (a), (c) and (e) were taken using the UAV system, and (b), (d) and (f) were taken using a camera from the ground. Images (a) and (b) are minimum-till corn-soybean rotation (MTCS) with no or low residue; (c) and (d) are no-till corn-soybean rotation (NTCS) with medium residue; and (e) and (f) are no-till continuous corn including cover crops (NTCC) with high residue. Images were acquired at 13 (MTCS and NTCS) or 14 (NTCC) days after planting.

corn seedlings from UAV imagery. The image processing method included three major steps of 1) developing a DL model for image segmentation; 2) pre-processing UAV image data to prepare the input images for the DL model; 3) post-processing the segmented images from the DL model to obtain final segmented images with the background removed.

2.3.1. Development of the deep learning model

The DL model used in this study was the U-Net model, which is a type of convolutional neural network and was first introduced for image segmentation in biomedical applications (Livne et al., 2019; Ronneberger et al., 2015). Recently, it has been widely used in agricultural applications for segmenting and classifying plants, weeds, and ground straw coverage (Fawakherji et al., 2019; Kitano et al., 2019; Zhang et al., 2020; Zhao et al., 2019; Zhou et al., 2020). The U-net model is able to extract global features and context information from small-sized images and does not require a large training dataset (Zhou et al., 2020), making it feasible for this study. These features make it suitable for object segmentation with low resolution, uncertain size, and complex backgrounds (Zhang et al., 2020). Studies also showed that the image segmentation accuracy (pixel-to-pixel comparison) was higher as compared to other DL models such as SegNet (Fawakherji et al., 2019; Zhang et al., 2020).

In this study, the U-Net model was built using the 'unetLayers' function in Matlab (R2019b, MathWorks, Natick, MA, USA) with an encoder and a decoder as illustrated in Fig. 3. The encoder learned image features from input images, and reduced its dimension (width × height) by the max pool operation (2 × 2 filter size). The decoder identified the localization of the object-of-interest based on the corresponding reference feature map from the encoder part (depth concatenation). The depth concatenation also restored the image to its original dimension by up-convolution (2 × 2 filter size) and up-ReLU (Rectified Linear Unit) operations. The bridge section connected the encoder and decoder parts. All convolution operations had a filter size of 3 by 3, except for the final convolution layer before the output segmented image, which had a filter size of 1 by 1. The dropout operation selected a probability (0.5 in this study) at which input elements were dropped out randomly to prevent overfitting when training the neural network (Srivastava et al., 2014). Fig. 3a–g visualize some channels from the multi-channel feature map of the step-by-step image segmentation from the model. Training options as indicated in Table 2 were used.

2.3.2. Pre-processing UAV images

Ten UAV images were randomly selected from each CS to train the U-Net model for image segmentation. Images were rotated to ensure plant rows were vertical based on visual inspection. Each plant row image was subsequently cropped to 200 pixels wide by the height of the rotated image (Fig. 4a–c) using Matlab (R2019b, MathWorks, Natick, MA, USA). The image width of 200 pixels (equivalent to 60 cm based on the average GSD of 0.3 cm pixel^{-1}) was selected to include one corn row in the middle and an adequate background. Then, smaller sized images with a dimension of 200 by 304 pixels were cropped from the plant row images, where the 304 pixels of image height covering 91 cm included one to five corn plants in each cropped image (Fig. 4d). Theoretically, five plants should have been included in the cropped images based on the 91 cm image length and plant spacing of 16 cm. However, the actual GSD changed during flight due to the variation of flight height caused by field slope and the error of UAV elevation sensor, resulting in fewer plants covered in some images. The cropped images were divided into training (70%), validation (20%), and testing (10%) datasets (Table 3). Training and validation datasets were used to build the DL model, and the model was evaluated using the testing dataset. Ground truth images (i.e.,

Table 2
Training option values used to train the model.

Training Option Name	Value
Solver	'adam'
Learning Rate	0.0001
Max Epoch	50
Mini Batch Size	64

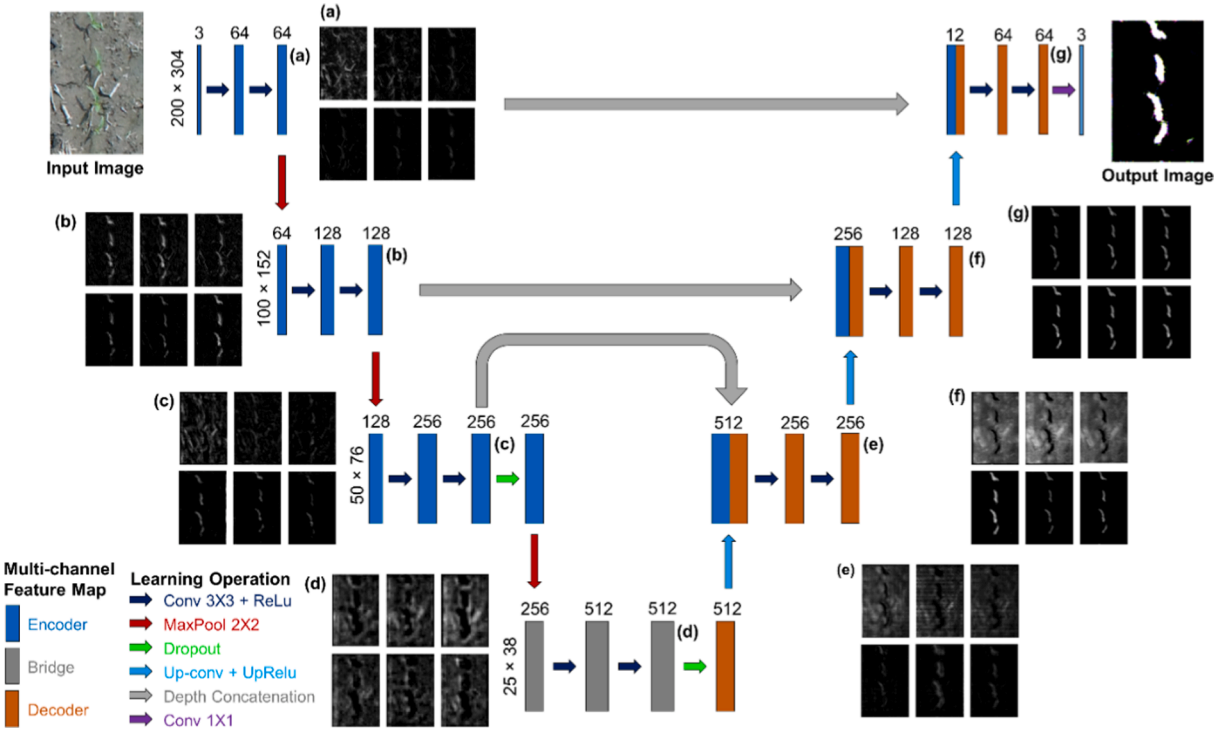

Fig. 3. The architecture of the U-net deep learning model used in the study with legend at the bottom left. Each rectangle represents a multi-channel feature map with the number of channels given above. Image dimension (width × height) is indicated at the left edge. (a) to (g) show example channels from the feature map.

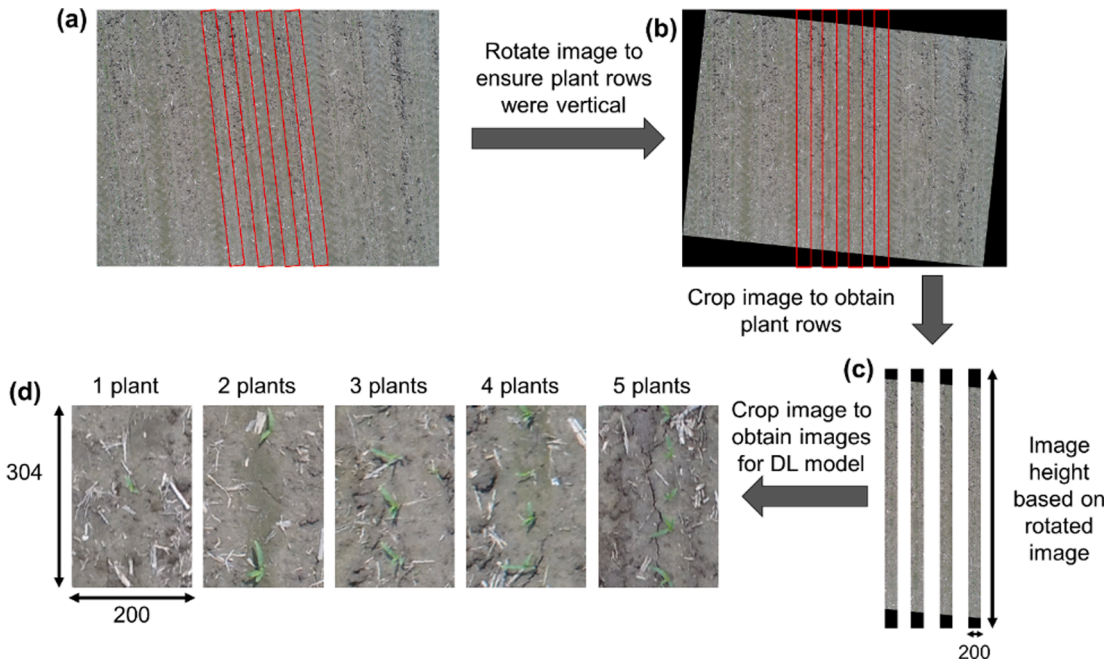

Fig. 4. Illustration of image data preparation for building the deep learning (DL) model in this study: (a) original UAV image where red boxes indicate plant rows; (b) rotated UAV image; (c) cropped images of plant rows; and (d) cropped images used to build DL model. (For interpretation of the references to color in this figure legend, the reader is referred to the web version of this article.)

Table 3
Number of cropped images from each cropping system used in training, validation and testing datasets.

Dataset	MTCS	NTCS	NTCC	Total
Training	1020	1000	1016	3036
Validation	290	280	288	858
Testing	140	130	139	409
Total	1450	1410	1443	

binary images of corn plants in white {pixel value = 1} and background in black {pixel value = 0}) of each cropped image were prepared using 'Image Segmenter' apps from the 'Image Processing and Computer Vision' toolbox in Matlab. Regions of interest (i.e., corn plants) were drawn using 'Draw ROIs' in the 'Image Segmenter' apps and the binary image was exported (Fig. 5j-l).

2.3.3. Post-processing segmented images from DL model

Followed by the U-Net model, image post-processing steps including an adaptive image thresholding method (Bradley and Roth, 2007) and the morphological operation of image erosion were used to remove the remaining background or any noise in the image (Fig. 5g-i). The final segmented binary image was compared with the ground truth binary image (Fig. 5j-l) to evaluate the image segmentation of the U-Net model using three parameters, namely precision, recall, and F1 (Table 4), which were computed by 'bfscore' in Matlab (Csurka et al., 2013). The average of each parameter for all the images in each CS as well as overall (for all CS) was calculated and reported.

2.4. Image processing workflow for plant stand count estimation

An image processing workflow (Fig. 6) was built to estimate plant stand count (number of plant m^{-1}) for each corn row. Firstly, UAV images were cropped to 4800 by 3648 pixels from the original dimension of 4864 × 3648 pixels using the 'imcrop' function in Matlab. This was done so that 288 images could be equally cropped from the UAV image to be used as input images in the U-Net model. The same DL model and post-processing steps as described previously (henceforth referred to as proposed method) were used to segment the cropped images. Then, the cropped images were combined sequentially, followed by a row detection step to prevent counting non-corn objects between rows (Fig. 6b–e). The row detection step began by first finding the lines (rows) in the binary image using a Hough transformation (Fig. 6c), and the angle detected was used to rotate the binary (Fig. 6d) and original images. When summing the number of pixels at each image width of the binary image ("1" for plants and "0" for background) and smoothing the data using a Gaussian filter, the detected peaks (red circles in Fig. 6e) represented each row (Varela et al., 2018). The image width position of each peak was used to crop each plant row from the rotated original image and binary image. Additionally, the plants in each row were manually counted using the original color image (Fig. 6f) and denoted as manual count. Likewise, the plants in the binary image (Fig. 6g) were counted by detecting the number of connected components in the image and denoted as UAV count. Since the corn plants were mostly in V2 or earlier growth stages, no plants overlapped. The exception to this was a small number of "double plants", caused by two seeds being released by the planter at the same time.

Seven to nine UAV images, comprised of about 60 plant rows for each CS were randomly selected for the manual and UAV corn stand count comparison in plants m^{-1}. The stand count in each row was determined using the ratio of the total number of plants in the row to the row length. The GSD for each selected image was different due to the variability of actual flight height caused by the UAV launch location and field slope. Thus, actual GSD (cm $pixel^{-1}$) was first calculated using the division of constant planter row spacing (76 cm) by row spacing in pixels from the image. The computed GSD ranged from 0.14 to 0.26 cm $pixel^{-1}$ for the UAV images used in the analyses. Then, the row length was determined by multiplying the number of pixels by the computed GSD. Lastly, scatter plots were created to compare the manual and UAV count. Previous studies used several metrics to describe model performance in estimating stand count, including coefficient of determination (R^2, Gnadinger and Schmidhalter, 2017) and MAPE (Kitano et al., 2019). Thus, these two metrics were utilized to allow for comparison with previous studies, and an additional performance metric of root-mean-

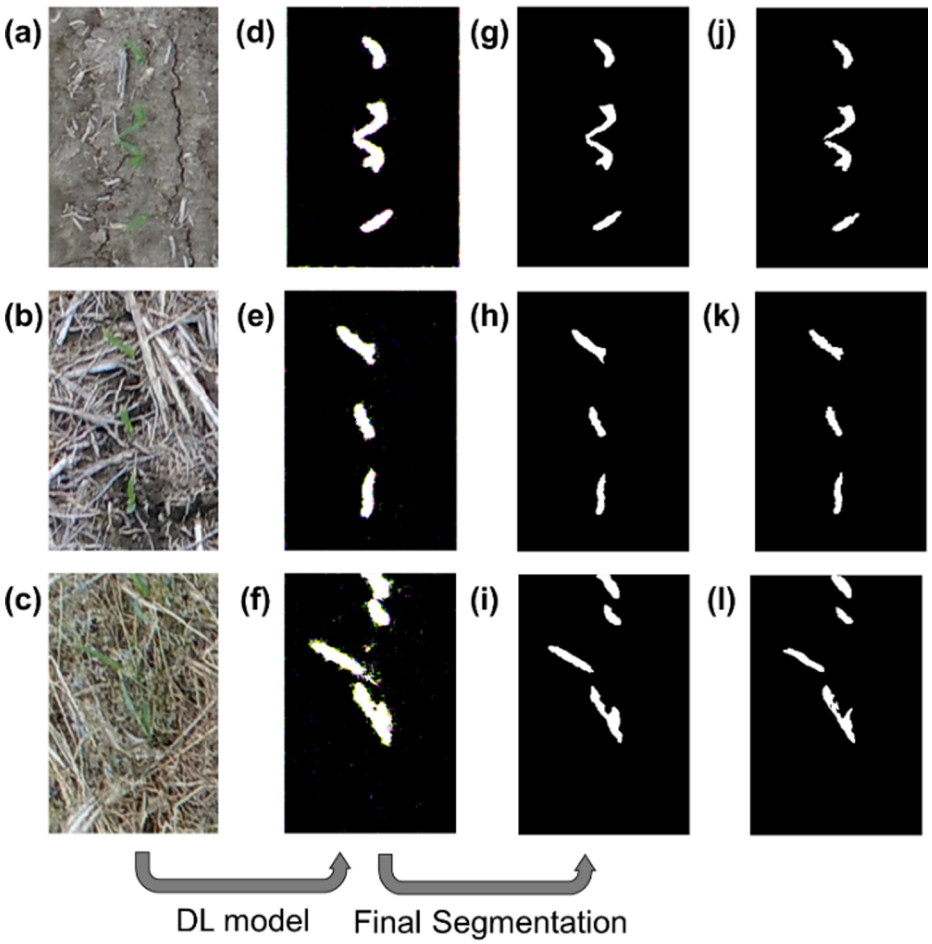

Fig. 5. Illustration of image segmentation using the proposed deep learning (DL) model and final segmentation results. Images (a) to (c) are the original images; (d) to (f) are output from the proposed DL model; (g) to (i) are final segmented images; (j) to (l) are ground truth binary images prepared using the 'Image Segmenter' apps for each cropping system: minimum-tillage corn-soybean rotation (top row); no-till corn-soybean rotation (middle row); no-till continuous corn including cover crops (bottom row).

Table 4
Parameter used to evaluate image segmentation (Csurka et al., 2013).

Parameters	Description
Precision	$Precision = \frac{TP}{TP + FP}$ where TP = true positive, number of pixels on the ground truth segmentation boundary that are also on the predicted segmentation boundary; FP = false positive, number of pixels on the predicted segmentation boundary but not on the ground truth segmentation boundary
Recall	$Recall = \frac{TP}{TP + FN}$ where TP = true positive, number of pixels on the ground truth segmentation boundary that are also on the predicted segmentation boundary; FN = false negative, number of pixels on the ground truth segmentation boundary but not on the predicted segmentation boundary
F1	Measures how close the predicted boundary of an object matches the ground truth boundary. $F1 = \frac{2 \times precision \times recall}{recall + precison}$

square error (RMSE) was also computed.

3. Results and discussion

3.1. Image segmentation evaluation

Example images of different CS with different precision, recall, and F1 values are shown in Fig. 7. The overlay showed a very close agreement between boundaries when the values of all three parameters were equal to one (Fig. 7a). Precision values were low when the UAV prediction indicated more plant area than that of the ground truth (Fig. 7d), or detected other green objects (Fig. 7c) as indicated in the overlay by the green color. Meanwhile, recall values were low when a portion of a plant (Fig. 7e and f) or a complete small-sized plant (Fig. 7b) in the ground truth was not included in the prediction as shown in the purple color of the overlay.

Results using the proposed method are listed in Table 5, including the average precision, recall, and F1 of training, validation and testing datasets for each CS and all the CS (overall). The MTCS had the highest performance with the greatest average precision, recall, and F1 (0.93–0.96), followed by NTCS (0.85–0.93), and NTCC (0.74–0.90). Thus, performance of the proposed method decreased as residue cover increased. Overall, the proposed method was able to segment corn plants from the background in UAV images of different CS with high precision, recall, and F1 for all the datasets (0.86–0.92). The MTCS and NTCS had higher average recall than precision for all datasets, suggesting that most prediction images in these CS had plants with larger area than that of the ground truth images. Nonetheless, the additional area of plants in the ground truth images was usually on the edge of the plants (Fig. 7d), and likely did not negatively affect the accuracy of plant stand count estimation. The low precision value also indicated the possibility of detecting other green objects, such as weeds, that were usually found between rows and would cause an over-prediction of stand count. This issue could be addressed by including the row detection step (Fig. 6b–e) to avoid counting non-corn objects between rows.

The NTCC had higher average precision than recall, indicating that most of the prediction images had plants with smaller area than that of the ground truth images. The NTCC had the highest amount of residue, with some of the residue covering part of the plant leaves. Hence, this

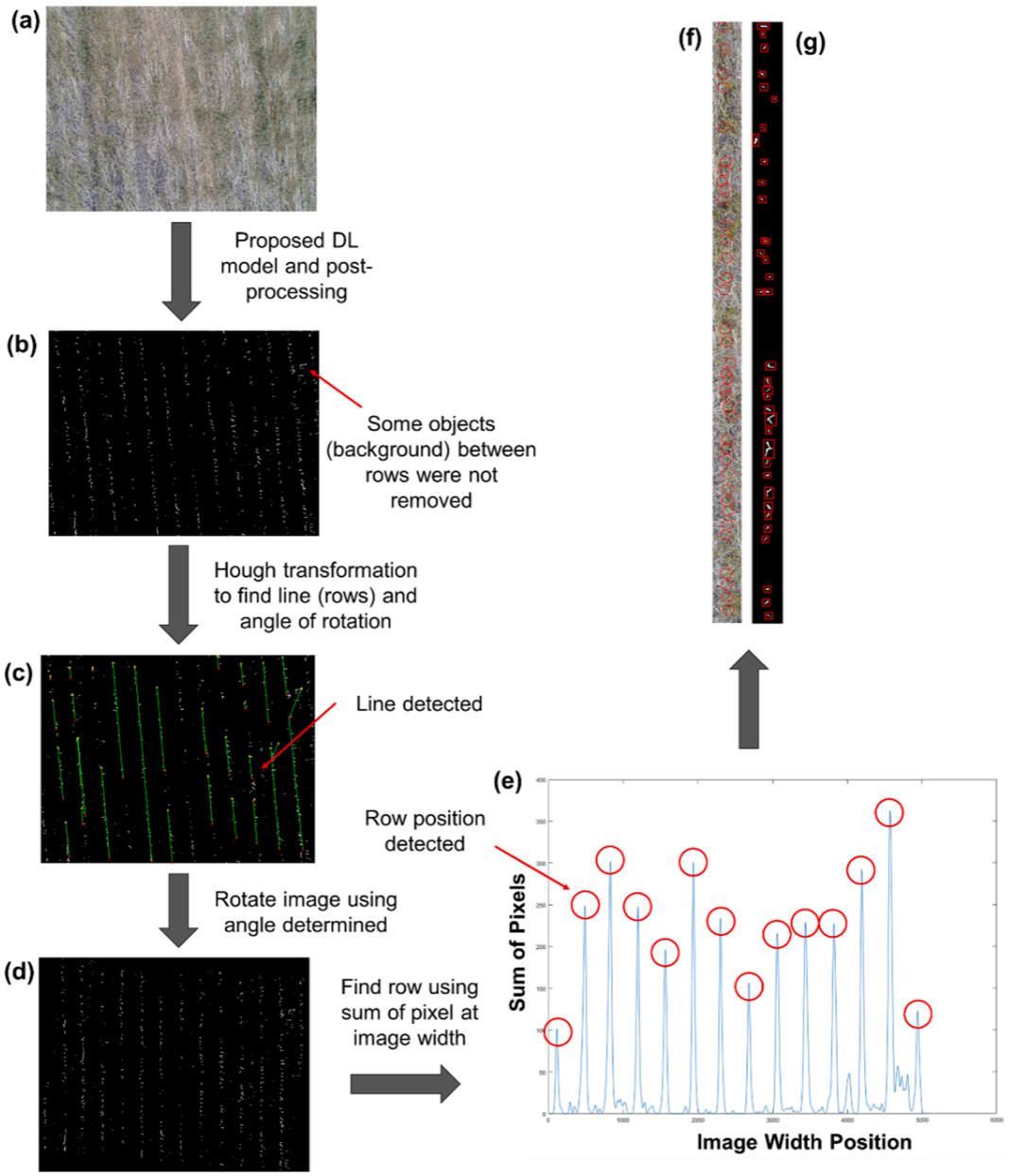

Fig. 6. Workflow of estimating plant population in each row of a single UAV image captured for the cropping system of no-till continuous corn including cover crops in this study. (a) original UAV image; (b) segmented binary image; (c) segmented binary image with lines in green found by Hough transformation; (d) rotated binary image; (e) smoothed curve with peaks representing plant row positions; (f) cropped original image for manual count (37 plants); (g) cropped binary image for UAV count (36 plants). (For interpretation of the references to color in this figure legend, the reader is referred to the web version of this article.)

covered part was not included in the prediction image (Fig. 7e and f). Additionally, low recall values could be caused by some plants not being detected, which would result in under-prediction during stand count estimation. This issue was especially apparent when the corn plants were surrounded by other green residue (i.e., plants not completely senesced after pre-plant herbicide application) in this NTCC CS, as illustrated in Fig. 8.

3.2. Plant stand count estimation

Nearly all the background was removed in images from MTCS and NTCS (Fig. 9). However, for NTCC, some of the background consisting of green residue was not completely removed (Fig. 9i and l). By introducing the additional step of row detection (Fig. 6b–e), these background objects were not included in the final cropped plant row image (Fig. 6f and g), thus improving the estimation accuracy. Good correspondence was observed between manual and UAV counts of corn for all the CS with R^2 of more than 0.9. (Fig. 10). The MTCS had the lowest RMSE and MAPE followed by NTCS and NTCC, suggesting that higher amounts of residue increased the difficulty of counting the correct number of plants.

The under-prediction in MTCS and NTCS was attributed to small-sized plants, which were late-emerging plants, and were considered as image noise and removed (Fig. 11a–d). Occasionally, the under-prediction was also due to the overlapped leaves of two close plants (“double plants”, Fig. 11e–h). On the contrary, over-prediction in MTCS and NTCS resulted from a limitation of the image processing workflow when the UAV image was cropped equally into 288 images. Some corn plants were split, with portions appearing in two images (Fig. 12a–d), and after the background removal using the proposed method followed by combining the images sequentially, the same plants were divided into two parts (Fig. 12e and f). For NTCC, higher amounts of residue resulted in more under- and over-prediction. These residues varied in color from

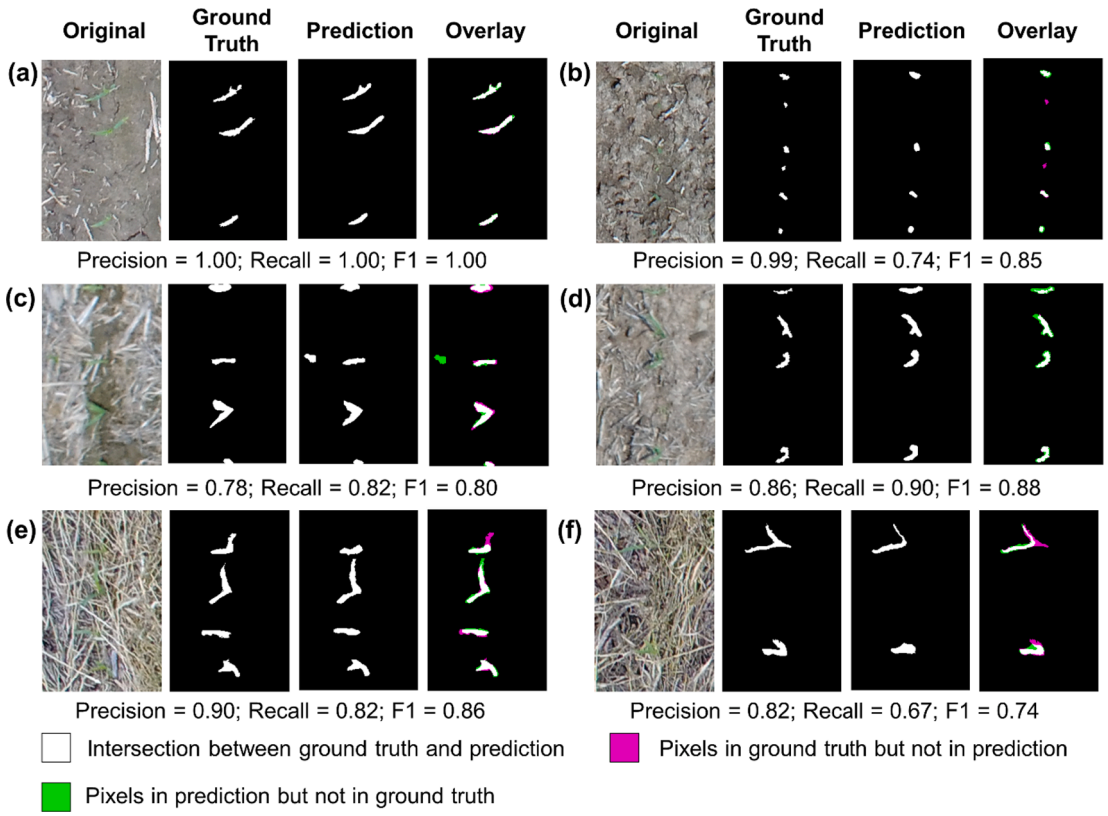

Fig. 7. Example images showing different precision, recall, and F1 values in three cropping systems: minimum-tillage corn-soybean rotation (a and b), no-till corn-soybean rotation (c and d), and no-till continuous corn including cover crops (e and f). 'Ground Truth' is the binary image prepared by 'Image Segmenter' apps, 'Prediction' is the segmented binary image from the proposed method, and 'Overlay' compares ground truth and segmented binary images.

Table 5
Average precision, recall and F1 of training, validation and testing datasets for different cropping systems.

Dataset	Parameter	MTCS	NTCS	NTCC	Overall
Training	Precision	0.95	0.89	0.90	0.91
	Recall	0.96	0.93	0.86	0.92
	F1	0.96	0.92	0.88	0.92
Validation	Precision	0.93	0.86	0.78	0.86
	Recall	0.94	0.92	0.74	0.86
	F1	0.94	0.90	0.74	0.86
Testing	Precision	0.94	0.85	0.81	0.87
	Recall	0.96	0.91	0.74	0.86
	F1	0.95	0.90	0.77	0.87

yellow or white dry straw (Fig. 13a) to yellow or light green cover crops or weeds (Fig. 13c). As indicated in Fig. 13a and b, some plants (red circle) were not detected, while in Fig. 13c and d, some plants (red box) were divided into two parts.

Although there was some under- and over-prediction for all the CS, our results show better or comparable performance of corn stand count estimation when compared to similar previous studies. For example, our results of $R^2 > 0.90$ for all the CS were higher than the R^2 of 0.89 in the study by Gnadinger and Schmidhalter (2017). Although neither the crop growth stage or CS were specificed, the UAV image shown in their article illustrated larger corn plants (3- to 5-leaves) with only soil background, which was comparable to the MTCS in the present study. Hence, the proposed method attained a higher performance at an earlier growth stage than this previous study.

Similarly, the MAPE results ranged from 4.51% to 16.57% across all

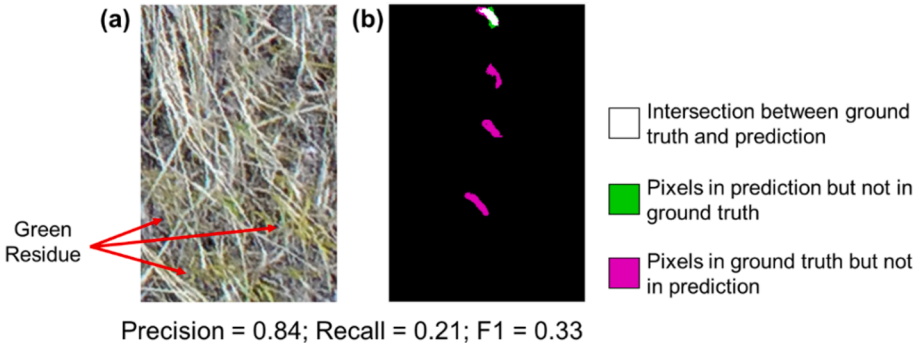

Fig. 8. Images showing a low recall value in the cropping system with no-till continuous corn including cover crops due to some plants that were not detected when surrounded by green residue. The original image is on the left (a) and the overlaid image between ground truth and segmented binary images is on the right (b). (For interpretation of the references to color in this figure legend, the reader is referred to the web version of this article.)

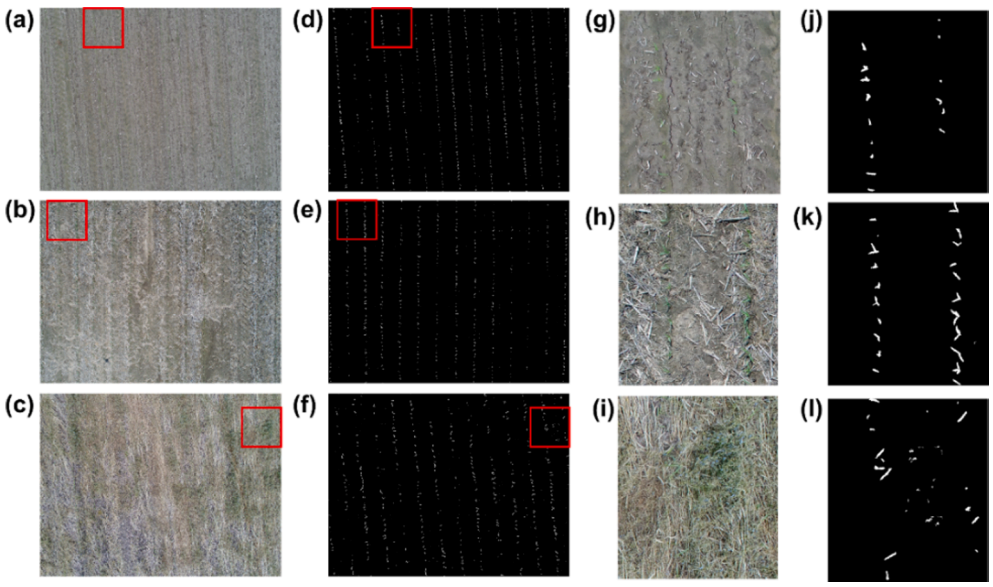

Fig. 9. Examples of UAV images from cropping systems: minimum-tillage corn-soybean rotation (top row), no-till corn-soybean rotation (middle row), and no-till continuous corn including cover crops (bottom row) used in plant stand count estimation. The original UAV images are in the first column (a–c) and segmented images using the proposed method are in the second column (d–f). Those parts of the original UAV and segmented images in the red boxes are enlarged and shown in the third and fourth columns (g–l). (For interpretation of the references to color in this figure legend, the reader is referred to the web version of this article.)

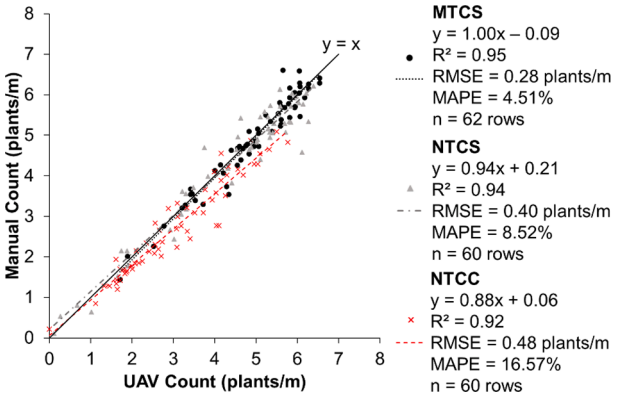

Fig. 10. Comparison between manual and UAV stand count for each cropping system: minimum-tillage corn-soybean rotation (MTCS), no-till corn-soybean rotation (NTCS), and no-till continuous corn including cover crops (NTCC).

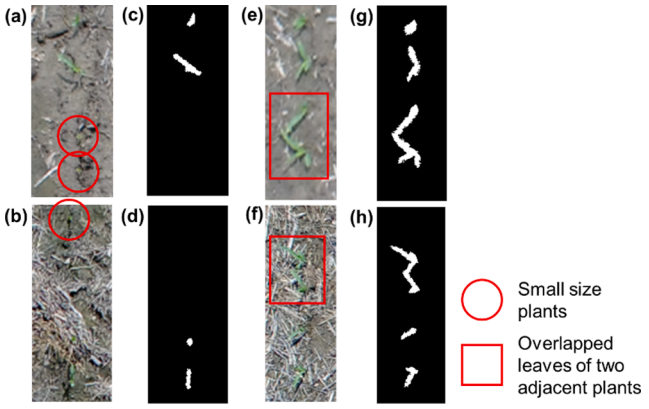

Fig. 11. Examples of original (a, b, e, and f) and segmented (c, d, g, and h) images showing under-prediction of plant stand count caused by small-sized plants (a-d) and overlapped leaves (e-h) for two cropping systems: minimum-tillage corn-soybean rotation (top row) and no-till corn-soybean rotation (bottom row).

CS. This showed comparable or better performance of the proposed method to results from previous research performed by Kitano et al. (2020), which found MAPE to range from 2.6 to 53.3%. They used DL and UAV images in estimating corn stand counts with different factors such as plant density (45,000, 70,000, and 90,000 plants ha^{-1}), flight height (10, 15, and 20 m), and vegetative growth stage (V4, V6, and V8). When considering the same flight height in our study (10 m), their MAPE ranged from 11.6 to 14.4% when estimating plant stand count at V4 stage. Although the NTCS in our study had MAPE of 16.57%, our proposed method was able to estimate the plant stand count at an earlier stage (V2 compared to V4, which is about 140 growing degree days earlier, Lee et al., 2007). Earlier detection of stand establishment could result in more time to implement management stragies, such as replanting.

Meanwhile, the RMSE in the present study was low for all the CS and ranged from 0.28 to 0.48 plants m^{-1} (Fig. 7a and b). A study by Shuai et al. (2019) estimated corn stand count at V2 (UAV images taken 25 DAP at 4 and 5 m flying height) in a field previously planted to wheat and tilled with a vertical tillage implement prior to corn planting. The UAV image in their paper illustrated only soil background, which was similar to MTCS. Their results showed that the model missed two to five plants per plot (129–141 plants) in six 5-m rows. An equivalent calculation based on RMSE from our research showed our proposed method missed eight plants per plot. The higher number of missing plants might have been caused by the lower spatial resolution of our study (3.0 mm pixel^{-1}) as compared to theirs (1.1 and 1.4 mm pixel^{-1}). Although our method provided a lower estimation accuracy, it was able to estimate corn stand 11 days earlier than this previous study (14 vs 25 DAP).

Overall, the proposed method was able to estimate early corn stand count (two weeks after planting, i.e. ~V2) for different CS with R^2 ranging from 0.92 to 0.95, RMSE of 0.28 to 0.48 plants m^{-1}, and MAPE of 4.51 to 16.57%. Further application of the proposed method could produce plant population maps of larger fields using stitched UAV images. This will potentially allow determining the exact location of areas of poor or no emergence in a field. As such, less time and labor will be needed as compared to traditional crop scouting methods.

4. Conclusion

This study proposed a method of using UAV imagery and a DL model in estimating early (V2) stand count of corn planted with different CS that varied in soil and residue backgrounds (MTCS, NTCS, and NTCC).

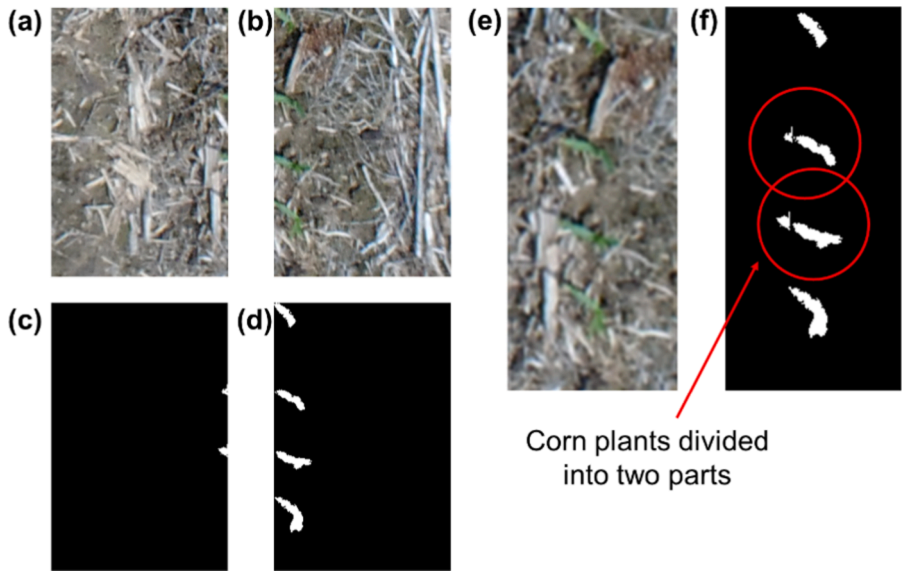

Fig. 12. Examples of original (a, b, and e) and segmented (c, d and f) images showing corn plants that were divided into two parts, resulting in over-prediction of plant stand count.

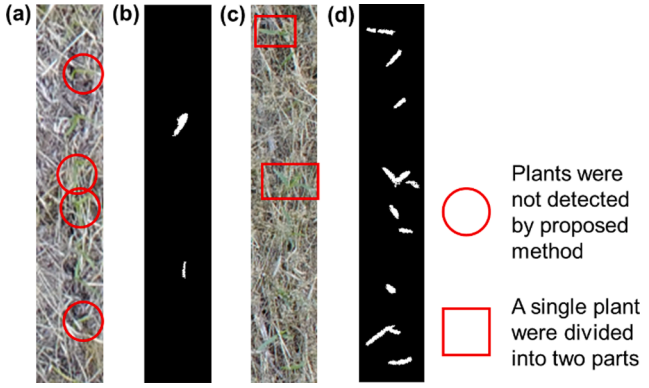

Fig. 13. Examples of original (a and c) and segmented (b and d) images showing under-prediction (a and b) and over-prediction (c and d) of plant stand count for the cropping system with no-till continuous corn including cover crops.

Results showed that plant identification by UAV imagery was more difficult as the complexity of the background increased with average precision of 0.94, 0.85, and 0.81 in the testing dataset for MTCS, NTCS, and NTCC CS, respectively. The proposed method using a U-Net DL model and image post-processing was able to remove the background from a UAV image and increase plant identification accuracy. For plant stand count estimation, the row detection step improved R^2 to >0.90 for all CS. Moreover, low RMSE (0.28–0.48 plants m^{-1}) and MAPE (4.51–16.57%) were attained for all the CS. The proposed method can be extended to estimate plant stand count for larger fields using stitched UAV images to produce plant population maps. These maps would be useful to researchers for making replanting decisions, estimating yield potential and nutrient recommendations, and evaluating effects of environmental factors on early emergence. To test the reliability of the proposed method, future validation work will be needed in plots and fields planted with similar or other soil and crop residue conditions.

CRediT authorship contribution statement

Chin Nee Vong: Methodology, Data curation, Formal analysis, Writing - original draft. **Lance S. Conway:** Investigation, Data curation, Writing - review & editing. **Jianfeng Zhou:** Supervision, Conceptualization, Data curation, Writing - review & editing. **Newell R. Kitchen:** Conceptualization, Investigation, Data curation, Resources, Writing - review & editing. **Kenneth A. Sudduth:** Conceptualization, Resources, Writing - review & editing.

Declaration of Competing Interest

The authors declare that they have no known competing financial interests or personal relationships that could have appeared to influence the work reported in this paper.

Acknowledgement

We would like to thank Dandan Fu, Jing Zhou, Aijing Feng, and Tianhua Li, members of the Precision and Automated Agriculture Lab at the University of Missouri for their assistance in UAV data collection. This research was partially funded by the US Department of Agriculture, Agricultural Research Service (project 5070-12610-005).

References

Albawi, S., Mohammed, T.A., Al-Zawi, S., 2017. Understanding of a convolutional neural network. In: Proceedings of International Conference on Engineering and Technology (ICET). https://doi.org/10.1109/icengtechnol.2017.8308186.

Amara, J., Bouaziz, B., Algergawy, A., 2017. A deep learning-based approach for banana leaf diseases classification. In: Datenbanksysteme für Business, Technologie und Web (BTW 2017) - Workshopband.

Assefa, Y., Vara Prasad, P., Carter, P., Hinds, M., Bhalla, G., Schon, R., et al., 2016. Yield responses to planting density for US modern corn hybrids: A synthesis-analysis. Crop Sci. 56 (5), 2802–2817. https://doi.org/10.2135/cropsci2016.04.0215.

Birrell, S., Sudduth, K.A., 1995. Corn population sensor for precision farming. ASAE Paper No. 951334. St. Joseph, Michigan: ASAE.

Bradley, D., Roth, G., 2007. Adaptive thresholding using the integral image. J. Graphics Tools 12 (2), 13–21. https://doi.org/10.1080/2151237X.2007.10129236.

Bollero, G.A., Bullock, D.G., Hollinger, S.E., 1996. Soil temperature and planting date effects on corn yield, leaf area, and plant development. Agronomy J. 88 (3), 385–390. https://doi.org/10.2134/agronj1996.00021962008800030005x.

Chen, R., Chu, T., Landivar, J.A., Yang, C., Maeda, M.M., 2018. Monitoring cotton (Gossypium hirsutum L.) germination using ultrahigh-resolution UAS images. Precision Agric. 19 (1), 161–177. https://doi.org/10.1007/s11119-017-9508-7.

Conway, L.S., Yost, M.A., Kitchen, N.R., Sudduth, K.A., Veum, K.S., 2018. Cropping system, landscape position, and topsoil depth affect soil fertility and nutrient buffering. Soil Sci. Soc. Am. J. 82 (2), 382–391. https://doi.org/10.2136/sssaj2017.08.0288.

Csurka, G., Larlus, D., Perronnin, F., Meylan, F., 2013. What is a good evaluation measure for semantic segmentation?. In: Proceedings of the British Machine Vision Conference (BMVC) https://doi.org/10.5244/C.27.32.

Fan, Z., Lu, J., Gong, M., Xie, H., Goodman, E.D., 2018. Automatic tobacco plant detection in UAV images via deep neural networks. IEEE J. Selected Topics Appl. Earth Observ. Remote Sensing 11 (3), 876–887. https://doi.org/10.1109/JSTARS.2018.2793849.

Fawakherji, M., Potena, C., Bloisi, D.D., Imperoli, M., Pretto, A., Nardi, D., 2019. UAV image based crop and weed distribution estimation on embedded GPU boards. In: Vento, M., et al. (Eds.) Computer Analysis of Images and Patterns. CAIP 2019. Communications in Computer and Information Science, vol. 1089. Springer, Cham. https://doi.org/10.1007/978-3-030-29930-9_10.

Ghosal, S., Zheng, B., Chapman, S.C., Potgieter, A.B., Jordan, D.R., Wang, X., et al., 2019. A weakly supervised deep learning framework for sorghum head detection and counting. Plant Phenom. 2019, 1525874. https://doi.org/10.34133/2019/1525874.

Gnadinger, F., Schmidhalter, U., 2017. Digital counts of maize plants by unmanned aerial vehicles (UAVs). Remote Sensing 9 (6), 544. https://doi.org/10.3390/rs9060544.

Guo, W., Zheng, B., Potgieter, A.B., Diot, J., Watanabe, K., Noshita, K., et al., 2018. Aerial imagery analysis–quantifying appearance and number of sorghum heads for applications in breeding and agronomy. Front. Plant Sci. 9, 1544. https://doi.org/10.3389/fpls.2018.01544.

Hobbs, P.R., Sayre, K., Gupta, R., 2008. The role of conservation agriculture in sustainable agriculture. Philos. Trans. R. Soc. B: Biol. Sci. 363 (1491), 543–555. https://doi.org/10.1098/rstb.2007.2169.

Jin, X., Liu, S., Baret, F., Hemerlé, M., Comar, A., 2017. Estimates of plant density of wheat crops at emergence from very low altitude UAV imagery. Remote Sensing Environ. 198, 105–114. https://doi.org/10.1016/j.rse.2017.06.007.

Kamilaris, A., Prenafeta-Boldú, F.X., 2018. Deep learning in agriculture: a survey. Comput. Electron. Agric. 147, 70–90. https://doi.org/10.1016/j.compag.2018.02.016.

Kitano, B.T., Mendes, C.C., Geus, A.R., Oliveira, H.C., Souza, J.R., 2019. Corn plant counting using deep learning and UAV images. IEEE Geosci. Remote Sensing Lett. https://doi.org/10.1109/lgrs.2019.2930549.

Lee, C., Herbek, J., Green, J.D., Martin, J., 2007. Replanting Options for Corn. Kentucky Cooperative Extension, University of Kentucky, IN.

Livne, M., Rieger, J., Aydin, O.U., Taha, A.A., Akay, E.M., Kossen, T., et al., 2019. A U-Net deep learning framework for high performance vessel segmentation in patients with cerebrovascular disease. Front. Neurosci. 13 https://doi.org/10.3389/fnins.2019.00097.

Nielsen, R.L., 2003. Estimating yield and dollar returns from corn replanting. AY-264-W. Lafeyette, IN: Purdue University Cooperative Extension Service, Purdue University.

Nunes, M.R., van Es, H.M., Schindelbeck, R., Ristow, A.J., Ryan, M., 2018. No-till and cropping system diversification improve soil health and crop yield. Geoderma 328, 30–43. https://doi.org/10.1016/j.geoderma.2018.04.031.

Pittelkow, C.M., Liang, X., Linquist, B.A., Van Groenigen, K.J., Lee, J., Lundy, M.E., et al., 2015. Productivity limits and potentials of the principles of conservation agriculture. Nature 517 (7534), 365–368. https://doi.org/10.1038/nature13809.

Ronneberger, O., Fischer, P., Brox, T., 2015. U-net: Convolutional networks for biomedical image segmentation. Proceedings of the International Conference on Medical Image Computing and Computer-Assisted Intervention (MICCAI).

Sadler, E.J., Lerch, R.N., Kitchen, N.R., Anderson, S.H., Baffaut, C., Sudduth, K.A., Prato, A.A., Kremer, R.J., Vories, E.D., Myers, D.B., Broz, R., Miles, R.J., Young, F., 2015. Long-term agro-ecosystem research in the Central Mississippi River Basin: Introduction, establishment, and overview. J. Environ. Quality 44 (1), 3–12. https://doi.org/10.2134/jeq2014.11.0481.

Sangoi, L., 2001. Understanding plant density effects on maize growth and development: an important issue to maximize grain yield. Ciência Rural 31 (1), 159–168. https://doi.org/10.1590/s0103-84782001000100027.

Shuai, G., Martinez-Feria, R.A., Zhang, J., Li, S., Price, R., Basso, B., 2019. Capturing maize stand heterogeneity across yield-stability zones using unmanned aerial vehicles (UAV). Sensors 19 (20), 4446. https://doi.org/10.3390/s19204446.

Stanger, T.F., Lauer, J.G., 2006. Optimum plant population of Bt and non-Bt corn in Wisconsin. Agronomy J. 98 (4), 914–921. https://doi.org/10.2134/agronj2005.0144.

Sudduth, K.A., Birrell, S.J., Krumpelman, M.J., 2000. Field evaluation of a corn population sensor. Proceedings of the International Conference on Precision Agriculture (ICPA).

Thorp, K.R., Steward, B.L., Kaleita, A.L., Batchelor, W.D., 2007. Using aerial hyperspectral remote sensing imagery to estimate corn plant stand density. Trans. ASABE 51 (1), 311–320. https://doi.org/10.13031/2013.24207.

Trujillano, F., Flores, A., Saito, C., Balcazar, M., Racoceanu, D., 2018. Corn classification using Deep Learning with UAV imagery. An operational proof of concept. In: Proceedings of the IEEE 1st Colombian Conference on Applications in Computational Intelligence (ColCACI). https://doi.org/10.1109/colcaci.2018.8484845.

Varela, S., Dhodda, P., Hsu, W., Prasad, P., Assefa, Y., Peralta, N., et al., 2018. Early-season stand count determination in corn via integration of imagery from unmanned aerial systems (UAS) and supervised learning techniques. Remote Sensing 10 (2), 343. https://doi.org/10.3390/rs10020343.

Van Roekel, R.J., Coulter, J.A., 2011. Agronomic responses of corn to planting date and plant density. Agronomy J. 103 (5), 1414–1422. https://doi.org/10.2134/agronj2011.0071.

Yost, M.A., Kitchen, N.R., Sudduth, K.A., Sadler, E.J., Baffaut, C., Volkmann, M.R., Drummond, S.T., 2016. Long-term impacts of cropping systems and landscape positions on claypan-soil grain crop production. Agronomy J. 108 (2), 713–725. https://doi.org/10.2134/agronj2015.0413.

Zhang, J., Xie, T., Yang, C., Song, H., Jiang, Z., Zhou, G., et al., 2020. Segmenting purple rapeseed leaves in the field from UAV RGB imagery using deep learning as an auxiliary means for nitrogen stress detection. Remote Sensing 12 (9), 1403. https://doi.org/10.3390/rs12091403.

Zhao, B., Zhang, J., Yang, C., Zhou, G., Ding, Y., Shi, Y., et al., 2018. Rapeseed seedling stand counting and seeding performance evaluation at two early growth stages based on unmanned aerial vehicle imagery. Front. Plant Sci. 9, 1362. https://doi.org/10.3389/fpls.2018.01362.

Zhao, X., Yuan, Y., Song, M., Ding, Y., Lin, F., Liang, D., Zhang, D., 2019. Use of unmanned aerial vehicle imagery and deep learning unet to extract rice lodging. Sensors 19 (18), 3859. https://doi.org/10.3390/s19183859.

Zhou, D., Li, M., Li, Y., Qi, J., Liu, K., Cong, X., Tian, X., 2020. Detection of ground straw coverage under conservation tillage based on deep learning. Comput. Electron. Agric. 172, 105369 https://doi.org/10.1016/j.compag.2020.105369.

Zhuang, S., Wang, P., Jiang, B., 2018. Segmentation of green vegetation in the field using deep neural networks. In: Proceedings of the World Congress on Intelligent Control and Automation (WCICA). https://doi.org/10.1109/wcica.2018.8630376.